Air cushion Barge Platform for Offshore Wind Turbine and its Stability at a Large Range of Angle

Hongbin Hao[a], Zhiqun Guo[a], Qingwei Ma[b,a], Guochun Xu[c]

[a] College of Shipbuilding Engineering, Harbin Engineering University, Harbin, Heilongjiang, China
[b] School of Engineering and Mathematical Sciences, City University of London, London, UK
[c] College of Maritime, Ningbo University, Ningbo, Zhejiang, China

Abstract

One of typical bases for floating offshore wind turbines is the barge platform that has merits of simpler structure and lower costs, but disadvantages of significant responses in waves. In order to improve the hydrodynamic performance of the barge platforms, in this paper a novel Air cushion Barge Platform (ACBP) is proposed, into which multiple air chambers are incorporated to mitigate the wave loads and reduce the dynamic motions due to waves. However, there is a lack of analytical tools that can evaluate the stability of the ACBP with multi-air cushions at large angles. To address this issue, an analytical method is developed for evaluating the stability of the ACBP in the whole range of trim angles, including very large angles with possible emergence of the platform bottom and so with air leakage from a few chambers before capsized. The newly proposed analytical method is calibrated by the CFD results, and then is employed for investigating the static and dynamic stability of the ACBP for a typical design.

Keywords: Offshore Wind Turbine (OWT); Air cushion Barge Platform (ACBP); Stability performance; Large angle

1. Introduction

There are two main types of offshore wind turbines (OWT): the fixed OWT and the floating one. In general, the fixed one works in shallow water or moderate deep water (e.g. less than 50m), but its cost increases very quickly with the water depth. The floating one is generally employed in the deep water. Because the floating one can be built and assembled in the shipyard, and then be towed to the working sea, its cost is not very sensitive to the water depth.

The wind energy in deep seas is more plentiful and steady than at near shore seas. Moreover, in deep seas the wind turbines have less impact on human activities. So it can be predicted that the wind energy exploitation will gradually moves to the deep seas, where the floating supporting platforms are more suitable for the OWT. There are mainly four types of supporting platforms for floating OWT (FOWT): spar-buoy, tension-leg platform (TLP),

semi-submersible platform and barge [1]. It is considered that the water depth for spar-buoy platform should be more than 100m [2] and 70m for TLP. The semi-submersible platform and barge do not have special requirement for water depth, but the barge is more adaptable to relatively shallower water depth. Besides, the barge has simpler structure, which makes it possible to be built using low-cost concrete. However, the seakeeping motion of the barge in large waves is more significant than the semi-submersible one [3]. Nonetheless, it can be improved by the high cost-effective passive damping systems.

There are mainly four types of passive damping systems: Tuned Liquid Column Damper (TLCD), Tuned Mass Damper (TMD), Open-bottom Tank (OBT) and Heave Bottom Plate (HBP) [4]. It was found that the TLCD and TMD can considerably reduce the pitch motion [5-9], and the OBT and HBP can effectively reduce the pitch but also the heave motions [10]. The OBT is more suitable, because it is more economically attractive, and the air cushion trapped in the OBT can reduce the wave loads as well as the bending moment acting on whole structures. Pinkster et al. experimentally and numerically studied the behavior of a large air-supported mobile offshore base, which shows that the midship bending moment can be reduced by air cushion [11]. Kessel studied the effect of air cushion division on the structural load of large floating offshore structures, and a significant reduction of bending moment was obtained [12].

Besides, the air cushion can provided buoyancy to reduce the draft, which is very beneficial for the transportation of the FOWT through shallow water. It has been known for a long time that the air cushion was used to increase the buoyancy of bottom-founded structures, which can reduce the draft of structure to allow transportation over a shallow water area [13-15].

The OBT has internal water free surface and trapped air above it, and so the structures with OBT are also called air cushion or air supported floating structures (ASFS). The water inside the structure is connected to the water outside. The internal free surface and trapped air bring difficulties to stability analysis.Although it is similar to damaged ships in the sense that the internal and external water is connected, the air above the internal free surface is assumed to be open to the atmosphere [16] for stability analysis of damaged ships. Therefore, the well-developed methods for analyzing damaged stability of ships cannot be used for the stability analysis of the ASFS.

Nonetheless, some efforts have been devoted to evaluating the stability of the ASFS literature. Bie at al. studied the static stability of air floated structures consisting of three small buoys, and an air-floating force reduction factor is put forward to embody the differences

between the air floated structures and ordinary floating structures in buoyancy variations [17][18]. They assumed that the buoys are axisymmetric and small in diameter with thin walls, and that the solid parts of the structure always submerge in water without air leakage, implying that the trim or heeling angle are limited. Ding et al. considered the case with multiple air cushions in one floating body and studied the towing motion characteristics of composite bucket foundation for OWT [19]. They gave some idea about how to calculate the stability but did not give enough details. Their focus was the motions of CBF which just needs initial stability properties. Liu et al. [20-21] studied a similar air cushion structure to that in [17], and gave only the properties of initial stability. Chenu at al. [22] presented their experimental investigations on initial stability of a structure with two air chambers, complementing to that studied by Pinkster et al [11]. Thiagarajan [23] dedicated their study on the stability of a multi-chamber air cushion structure with a thin wall at the small trim and heeling angles by linearizing the pressure expression in air cushion. Kessel[24] presented the air cushion supported structures numerically and experimentally. In the work, they described the principle for analyzing large angle on stability in term of air cushion reduction factor but gave only its expression for small angle or displacement, without the results for righting moment at large angles. Their theory did not consider possible air escaping from underneath the structure at large trim or heeling angle like in [17].

In summary, most publications for the air cushion supported structures with multi air chambers studied only their initial stability (i.e., small trim or heeling angles), a few gave some idea about analyzing the stability without results at large angles, but none has considered the stability at very large angles with a possibility of emergence of structural bottom and so leakage of air. In practice, one should consider the static and dynamic stability of the structures during design. For analyzing the dynamic stability, one does need the righting moment in the whole range of trim or heeling angles until capsized.

In this paper, we will present a method and corresponding equations for analyzing the stability of a structure with multi-air cushions, the ACBP, in the whole range of trim or heeling angles, including the air leakage from a few air chambers before capsized.The principle may also be applied to other types of air cushion structures.For ease of discussions, the concept of the ACBP was presented firstly. Then an analytical method was developed for evaluating the stability of the ACBP with validation by CFD calculating results. Finally the stability properties of the ACBP were investigated.

2. Concept of ACBP

Many researchers have investigated the concepts or stabilities of OBT and ASFS. Typical works are as follows. Ma and Patel have incorporated 8 OBTs into a spar platform, in which the water columns can flow in and out through open bottoms and the trapped air above water columns acts as a spring [25]. Bie et al. [26], Chenu at al. [22] and Kessel[24] found that, if the platform is completely supported by a large single air cushion, the stability will deteriorate due to the fact that the relative center of buoyancy is not shifted when the platform heels. It can be improved by increasing the thickness of vertical walls around the air cushion or subdividing the air cushion into multiple compartments.

In this paper, a new structure named Air cushion Barge Platform (ACBP) was presented for offshore wind turbines, which is formed by incorporating the subdivided air chambers and a ballast tank onto a barge, as shown in Figure 1. The barge platform and the ballast tank are connected by a truss (see Figure 1a), which is similar to the structure of the Truss-Spar platform. The barge platform consists of a buoyancy tank, internal air chambers and a central moon pool (Figure 1b). The air chambers uniformly distribute around the central moon pool (Figure 1c). Moreover, the bottom of the buoyancy tank was equipped with a damping plate to increase the heave damping and reduce the heave response.

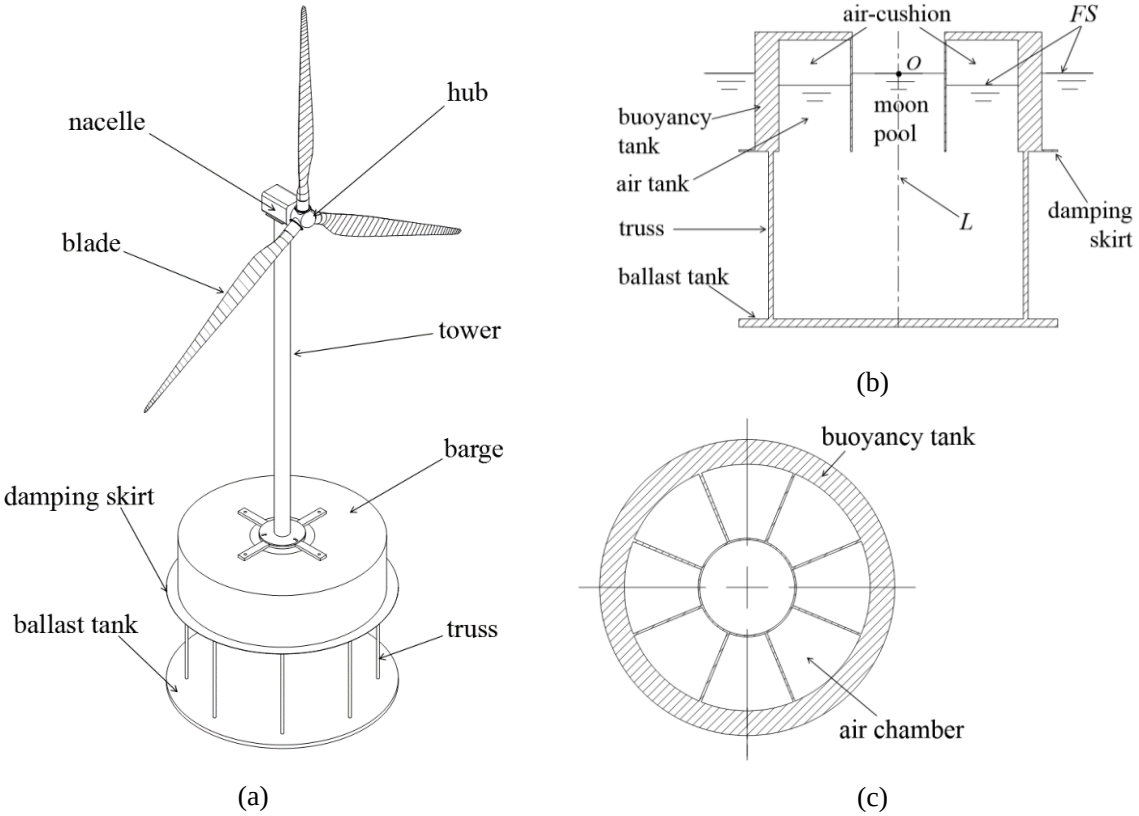

Figure 1. The sketch of Air cushion Barge Platform (ACBP)

The buoyancy tank is the main part of the barge platform, which provides the main buoyancy for the system. The air in the chambers plays the role of air springs to mitigate the wave loads and reduce the motion response. Obviously, the air chambers can provide positive buoyancy if the water level in air chambers is lower than the external one. Inversely, the buoyancy is negative if the water level in air chambers is higher than the latter.

The ballast tank can help lowering the center of gravity (COG) and so increasing the stability performance. Besides, the ballast tank can also play the function of damping plate to increase the heave damping and reduce the heave response.

The barge platform can climb up and down along the truss with the help of hoisting equipment. As a result, the drought of the ballast tank can be adjusted to adapt to the water depth, which makes the ACBP be possible to be transported through the shallow water as whole after built and assembled in shipyard, helping reducing installation time on site and costs. The conceptional design parameters are shown in Table 1.

Table 1. The principal parameters of the ACBP

Internal radius of air cushion R_1	5.6 m	Installed draft	20.0 m
External radius of air cushion R_2	14.0 m	Buoyancy tank draft d	6.18 m
External radius of buoyancy tank R_3	18.0 m	Number of air chambers	8
Radius of ballastR_4	20.0 m	Ballast mass	2,000,000 kg
Radius of damping skirt	20.0 m	Total mass	2,704,000 kg
Deck clearance z_{f0}	4.0 m	COG of ACBP	(0.0, 0.0, -14.65) m
Free Surface in air cushion z_{a0}	0.0 m	COG of ACBP-OWT	(0.0, 0.0, 1.468) m

*COG is the center of gravity

Table 2. The principal parameters of the NREL-5MW Offshore Wind Turbine (OWT)

Rotor orientation, configuration	Upwind, 3 Blades	Rotor diameter D_{rotor}	126m
Rated tip speed $V_{tip\text{-}R}$	80m/s	Hub diameter D_{hub}	3m
Hub height H_{hub}	90 m	Cut-in wind speed V_{in}	3m/s
Rotor mass m_{rotor}	110,000 kg	Rated wind speed V_{rated}	11.4m/s
Nacelle mass $m_{nacelle}$	240,000 kg	Cut-out wind speed V_{out}	25m/s
Tower mass m_{tower}	347,460 kg	Cut-in rotor ω_{in}	6.9rpm
Overall COG location G_{COG}	(-0.2, 0.0, 64.0) m	Rated rotor ω_{rated}	12.1rpm

For this conceptional design, the NREL-5MW Offshore Wind Turbine (OWT) is selected. For simplicity, the combined system of the NREL-5MW OWT and ACBP is called ACBP-OWT. The main parameters of the NREL-5MW OWT is shown in Table 2 [27-28].

Other turbines may be employed with different parameters.

Obviously, the stability performance of the ACBP-OWT is vital and must be evaluated carefully. However, the air cushion makes the problem very complex and different from conventional ones due to the following facts.

1) The righting moment is provided by the buoyancy of structure and air cushion, which might affect each other.

2) The compressibility of the air cushion makes their displacement vary.

3) The shape of immersion volume can be very complicated at large heeling/trim angles due to the possibility that the wet deck or free board is immersed into water.

4) Some air chambers might open to atmospheres at large heeling/trim angles, and suddenly completely lose the buoyancy, but others still submerge in water.

The stability of ACBP-OWT is similar to the second and third type of damage stability in ships, but there exist some significant differences. In ships' damage stability, the air above the internal free surface is assumed to be open to the atmosphere, so the well-developed theories of damage stability in ships cannot work for analyzing the stability of ACBP-OWT.

There are some stability theories of air-cushion supported floating structures, but they cannot analyze the stability performance of ACBP-OWT adequately. Firstly, the existing methods aims to analyzing the initial stability at little trim angles, which may be invalid at large trim angles due to the strong nonlinear effects. Secondly, the intercoupling between structure and air-cushion is not appropriately taken into account, and it should be analyzed appropriately when ACBP-OWT locates at large trim angles. Thirdly, the righting moment in the whole range of trim until capsized will be studied, and the structural bottom will emerge at very large angles and the air leakage cannot be ignored, which is not considered in previous studies. Lastly, the shape of air-cushion in ACBP-OWT is very complicated, which make it difficult calculate the center of gravity and buoyancy. Thereby, the existing stability methods cannot be directly used for analyzing the stability of ACBP-OWT, and a new stability analysis method will be developed for this novel system.

3. Theoretical analysis of stability

According to the above discussions, the existing stability methods cannot be directly applied to the ACBP-OWT, so we need to develop a new stability analysis method. The righting moment of the system can be divided into two parts for any given trim angle, that is

$$M_R = M_A + M_S \tag{1}$$

where M_A is the contribution of air cushion, M_S the contribution due to the displacement and

weight of structures,which is made up by the contribution of buoyancy tank, ballast tank and gravity, that is

$$M_S = M_{BT} + M_{bal} + M_g \tag{2}$$

Where M_{BT} and M_{bal} are the moment of buoyancy provided, respectively, by the buoyancy tank and the ballast tank, and M_g is the moment of gravity.

On the other hand, the righting moment can be written as

$$M_R = F_R \cdot L_R \tag{3}$$

where F_R is the righting force and L_R is the arm of F_R. It is noted that the wetted volume and shape of structures may be different at different trim/heeling angles and so the above components of moments are dependent on each other, which cannot be estimated separately.

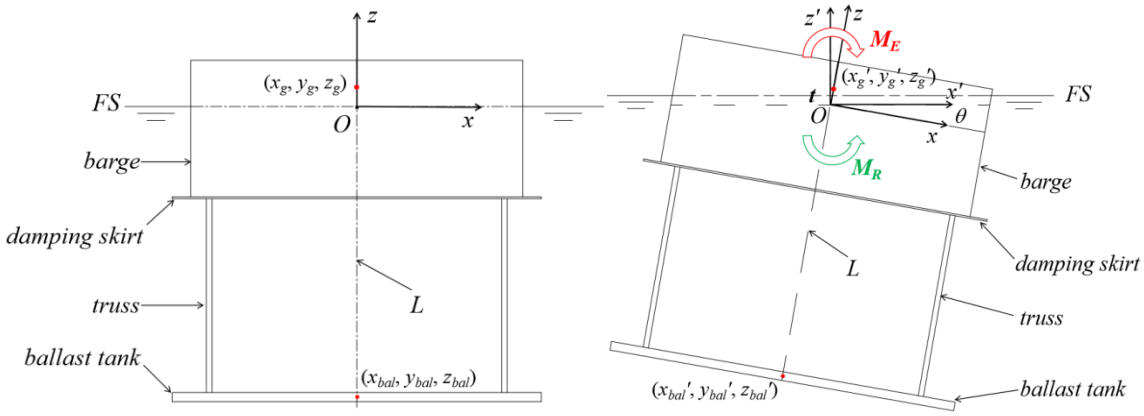

(a) (b)

Figure 2. Definition of the coordinate systems

Since the ACBP is symmetric about the horizontal axes, only trim and sinkage are investigated in this paper, though the method can be extended to consider more general cases. As shown in Figure 2a, the ACBP-OWT floats vertically at undisturbed floating state without any angle.*L* is its center line and intersects with free surface (FS) at Point *O*. Let *O-xyz* be the body-fixed coordinate system. At the undisturbed floating state, *x*-axis is the horizontal axis pointing to the right direction, and *z*-axis is the vertical axis pointing upwardly. Let *O-x'y'z'* be the accompanied coordinate system, which is parallel to *O-xyz* at the undisturbed floating state, and always shares the same origin as the *O-xyz* but does not rotate with it as indicated in Figure 2b.

If an external moment M_E is applied to the system, the ACBP-OWT will move to a new floating state, in which the righting moment M_R can balance the external M_E, as shown in Figure 2b at an angle. In the *O-xyz* coordinate system, let (x_g, y_g, z_g) be the COG of the ACBP-OWT and (x_{bal}, y_{bal}, z_{bal}) be the centroid of ballast tank. In the defined coordinate

system, $x_g=y_g=x_{bal}=y_{bal}=0$, let θ be the trim angle of the system at the new equilibrium state under action of the external moment. Then M_{bal} and M_g can be obtained directly by

$$M_g = -mgx_g' = -mgz_g \sin\theta \tag{4}$$

$$M_{bal} = \rho g V_{bal} x_{bal}' = \rho g V_{bal} z_{bal} \sin\theta \tag{5}$$

where x_g' and x_{bal}' are the x-coordinate of the COG and the centroid of ballast tank in the O-$x'y'z'$ coordinate system, respectively; and V_{bal} the volume of ballast tank.

At the new equilibrium state, the positions of external and internal free surfaces are unknown. The details below will be given for finding them.

3.1 Equations for the relative positions of internal and external water surface at new equilibrium state

At the new equilibrium state, the system has an angle and also a sinkage relative to the undisturbed state, leading to different positions of internal and external water surfaces relative to the coordinate systems. At this state, two conditions should be satisfied. One is that the total buoyancy is constant. The other is that the ideal gas state equation is satisfied in every air chamber. There are three compression models for gas in air chamber, which are the isothermal process, isochoric process and adiabatic process. In isochoric process model, the air is considered incompressible that is used in the third type of damage stability. In this paper, the three compression models for gas in air chamber are all studied for the comparison purpose.

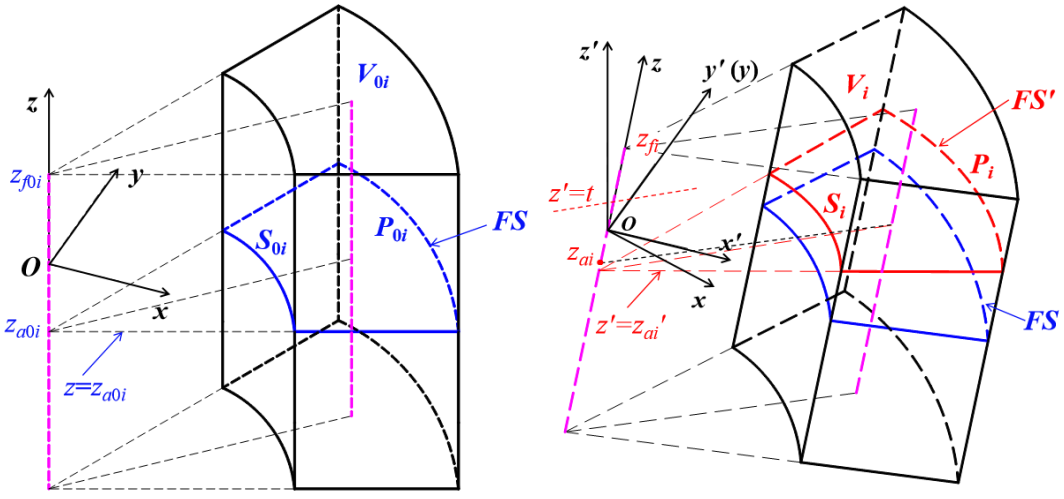

(a) (b)

Figure 3. Sketch of *i*th air chamber in undisturbed floating state and new equilibrium state

Let V_{0i} andP_{0i} be the volume and pressure, respectively, of the *i*th air chamber at undisturbed floating state (shown in Figure 3a); $V_i$and P_i be those at the new equilibrium state

(shown in Figure 3b), respectively. Then if no air leaks from the ith air chamber, one obtains

$$P_{0i}V_{0i} = P_iV_i \tag{6}$$

in which

$$V_{0i} = S_{0i} \cdot (z_{f0i} - z_{a0i}) \tag{7}$$

$$P_{0i} = P_a + \rho g(-z_{a0i}) \tag{8}$$

Where z_{f0i} and z_{a0i} are the z-coordinates of the centroid of the top surface of ith air chamber and the internal free surface in it, respectively; S_{0i} is the horizontal section area of ith air chamber, P_a the standard atmospheric pressure.

Let t and z_{ai}' be the z-coordinates of external and internal free surface in the O-$x'y'z'$ coordinate system, respectively, and z_{ai} be the z-coordinate of internal free surface centroid in the O-xyz coordinate system. Then V_i and P_i can be written as

$$V_i = S_{0i} \cdot (z_{f0i} - z_{ai}) \tag{9}$$

$$P_i = P_a + \rho g(-z_{ai}'+t) \tag{10}$$

where S_i is the area of internal free surface at the new equilibrium state and Eq. 9 will be proved later in Eq. 21.

Providing that the ballast tank is always under water, the sum of buoyancy from air chambers and buoyancy tank keeps constant, i.e.

$$\sum_{i=1}^{n} \Delta F_i + \rho g \cdot \Delta V_{BT} = 0 \tag{11}$$

where ΔV_{BT} is the increase of the displacement volume of the buoyancy tank, ΔF_i is the increase of buoyancy from ith air chamber and can be obtained from

$$\Delta F_i = (P_i - P_a) \cdot S_i - (P_{0i} - P_a) \cdot S_{0i} = \rho g(S_{0i} \cdot z_{a0i} - S_i \cdot z_{ai}'+S_i \cdot t) \tag{12}$$

Combining Eqs. 6-12, one can solve z_{ai} and t, and thus the new equilibrium state is obtained now.

3.2 Righting moment of the air cushion

At the undisturbed floating state, the sketch of the ith air chamber is shown in Figure 4, where $ABCD$ is the internal free surface and O_i its centroid, l_i the centre line that connects the centroid of the wetted surface and internal free surface. The horizontal cross-section of the internal free surface is shown in Figure 4b, where EF is the symmetric line of $ABCD$, φ_i the angle from Ox to OE, α_{1i} and α_{2i} the angles from OE to OB and OA, respectively.

Assuming that the internal and external radius of the ith air chamber is R_1 and R_2, respectively, the area of $ABCD$ can be calculated by

$$S_{0i} = S_{COD} - S_{AOB} = (\alpha_{2i} - \alpha_{1i})(R_2^{\ 2} - R_1^{\ 2})/2 \tag{13}$$

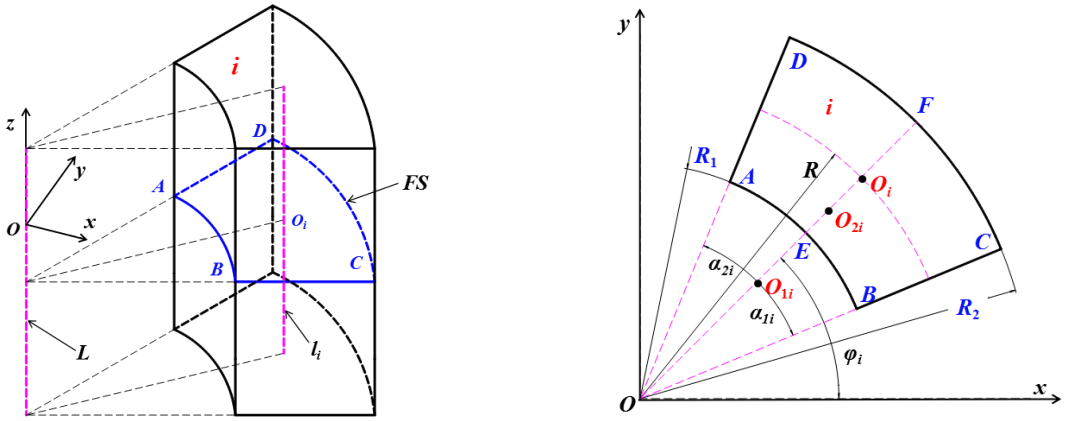

(a) (b)

Figure 4. Sketch of the *i*th air chamber

If O_{1i}, O_{2i} are the centroid of area *AOB*, *COD*, respectively, the distance from O_i to *L* is

$$R = OO_i = \frac{OO_{2i} \cdot S_{COD} - OO_{1i} \cdot S_{AOB}}{S_{0i}} = \frac{4(R_1^{\ 2} + R_2^{\ 2} + R_1R_2)\sin[(\alpha_{1i} - \alpha_{2i})/2]}{3(R_1 + R_2)(\alpha_{1i} - \alpha_{2i})} \tag{14}$$

in which, OO_{2i}=2R_2/3, OO_{1i}=2R_1/3.

At the new equilibrium state, the internal free surface moves to *A'B'C'D'*, as shown in Figure 5, in which the centroid is O_i*'*. For the convenience of analysis, the internal free surface *ABCD* and *A'B'C'D'* were enforced to move along the center line *L* untilz_{a0i} = 0 and z_{ai}*'* = 0, as shown in Figure 6, which does not falsify the conclusion. It is assumed that *P* and *P'* are points on *AB* and *A'B'*, respectively, and *PP'* is a line on surface *ABB'A'* that parallels to *AA'*.

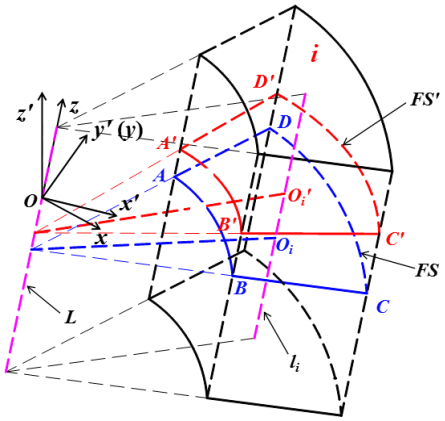

Figure 5. The sketch of the internal free surface at the new equilibrium state

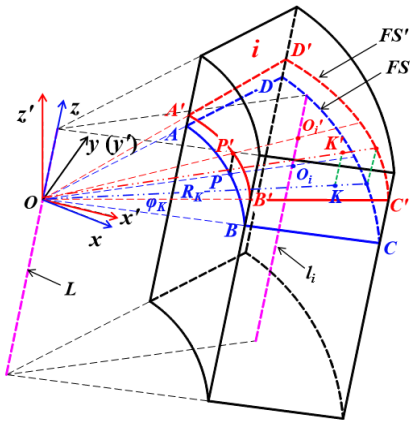

Figure 6. The sketch of the internal free surface that move to z_{a0i} = 0 and z_{ai}*'* = 0

In the *O-xyz* coordinate system, let (x_p, y_p, z_p) be the coordinate of *P*, φ_P be the angle from *Ox* to *OP*, α_{1P} and α_{2P}be the angles from *OP* to *OB* and *OA*, respectively, and then we have

$$x_P = R_1\cos\varphi_P,\quad y_P = R_1\sin\varphi_P,\quad z_P = 0,\quad \alpha_{2P} - \alpha_{1P} = \alpha_{2i} - \alpha_{1i}$$

Analogously, in the *O-x'y'z'* coordinate system, let ($x'_{P'}$, $y'_{P'}$, $z'_{P'}$) be the coordinate of *P'*, $\varphi_{P'}$ the angle from *Ox'* to *OP'*, and then according to the geometrical relationship we get

$$x'_{P'} = x_P/\cos\theta = R_1\cos\varphi_P/\cos\theta,\ y'_{P'} = y_P = R_1\sin\varphi_P,\quad z'_{P'} = 0$$

$$\varphi_P' = \arctan(y'_{P'}/x'_{P'}) = \arctan(\tan\varphi_P\cdot\cos\theta)$$

from which we obtain

$$\frac{x'^{\,2}_{P'}}{(R_1/\cos\theta)^2} + \frac{y'^{\,2}_{P'}}{R_1^{\,2}} = 1 \tag{15}$$

This is the equation of an ellipse, so *A'B'* is a segment of an ellipse. Let α_{1P}' and α_{2P}' be the angles from *OP'* to *OB'* and *OA'*, respectively, the area of *A'OB'* is

$$S_{A'OB'} = \int_{\varphi_P'+\alpha_{1P}'}^{\varphi_P'+\alpha_{2P}'} OP'^2\cdot\frac{1}{2}d\varphi_P' = \frac{1}{2}\int_{\varphi_P+\alpha_{1P}}^{\varphi_P+\alpha_{2P}}\frac{R_1^{\,2}}{\cos\theta}\cdot d\varphi_P = \frac{1}{2}\frac{R_1^{\,2}(\alpha_{2P}-\alpha_{1P})}{\cos\theta} \tag{16}$$

in which, $OP'^2 = x'^{\,2}_{P'} + y'^{\,2}_{P'}$, $d\varphi_P' = \dfrac{\cos\theta}{\cos^2\varphi_P + \sin^2\varphi_P\cdot\cos^2\theta}d\varphi_P$.

Thereby,

$$S_i = S_{C'OD'} - S_{A'OB'} = \frac{1}{2}\frac{(R_2^{\,2}-R_1^{\,2})(\alpha_{2P}-\alpha_{1P})}{\cos\theta} = \frac{1}{2}\frac{(R_2^{\,2}-R_1^{\,2})(\alpha_{2i}-\alpha_{1i})}{\cos\theta} = S_{0i}/\cos\theta \tag{17}$$

Eq. 17 shows that the area of *ABCD* is the projection of *A'B'C'D'*, which is the same to regular shapes.

According to the geometrical similarity,O_i must be on l_i and O_iO_i' is parallel to *PP'* and *AA'*. So O_iO_i' is parallel to l_i and O_i' should also be on l_i, which means that the centroid of internal free surface is always on the centre line of the *i*th air chamber.

In Figure 6, let *K* and *K'* be the points on surface *ABCD* and *A'B'C'D'*, and *KK'* is parallel to l_i. If $OK = R_K$, the angle from *Ox* to *OK* is φ_K, the volume of the bulk *ABCD-A'B'C'D'* can be obtained by the integral

$$\begin{aligned} V_{ABCD-A'B'C'D'} &= \iint_{ABCD} KK'\cdot dS = \int_{R_1}^{R_2}\int_{\varphi_i+\alpha_{1i}}^{\varphi_i+\alpha_{2i}} R_k\tan\theta\cos\varphi_k\cdot R_k\cdot d\varphi_k\cdot dR_k \\ &= (1/3)(R_2^{\,3}-R_1^{\,3})\cdot\tan\theta\cdot[\sin(\varphi_i+\alpha_{2i})-\sin(\varphi_i+\alpha_{1i})] \end{aligned} \tag{18}$$

in which, $KK' = R_k\cdot\tan\theta\cdot\cos\varphi_k$, $dS = R_k\cdot d\varphi_k\cdot dR_k$.

On the other hand, according to the geometrical relationship

$$S_0\cdot|O_iO_i'| = S_0\cdot R\cos\varphi_i\tan\theta = (2/3)(R_2^{\,3}-R_1^{\,3})\cdot\tan\theta\cdot\sin[(\alpha_{2i}-\alpha_{1i})/2]\cos\varphi_i \tag{19}$$

It can be proved by algebraic simplification that

$$2\sin[(\alpha_{2i}-\alpha_{1i})/2]\cos\varphi_i = \sin(\varphi_i+\alpha_{2i})-\sin(\varphi_i+\alpha_{1i})$$

One obtains

$$V_{ABCD-A'B'C'D'} = S_0 \cdot |O_i O_i'| = S_0 \cdot (z_{O_i'} - z_{O_i}) \tag{20}$$

It means the volume of this irregular shape with vertical side walls is equal to the area of vertical bottom surface multiply the distance of centroids between the bottom and top surface.So the volume of the *i*th air chamber at the new equilibrium state is

$$V_i = S_{0i} \cdot (z_{f0} - z_{ai}) \tag{21}$$

Besides, according to the geometrical relationship

$$-z'_{ai} / \cos\theta = -z_{ai} + R\cos\varphi_i \cdot \tan\theta \tag{22}$$

The buoyancy from the *i*-th air chamber is

$$F_i = (P_i - P_a) \cdot S_i = \rho g \cdot S_i \cdot (-z_{ai}' + t) = \rho g \cdot S_i \cdot (-z_{ai} \cdot \cos\theta + R\cos\varphi_i \cdot \sin\theta + t) \tag{23}$$

In the *O-xyz* coordinate system, the buoyancy center of F_i is

$$x_{iF} = R\cos\varphi_i, \quad y_{iF} = R\sin\varphi_i, \quad z_{iF} = [z_{ai} + R\cos\varphi_i \tan\theta + t/\cos\theta]/2$$

which can be expressed in the *O-x'y'z'* coordinate system as

$$x_{iF}' = x_{iF}\cos\theta + z_{iF}\sin\theta, \quad y_{iF}' = y_{iF}, \quad z_{iF}' = z_{iF}\cos\theta - x_{iF}\sin\theta$$

Therefore, the righting moment provided by the *i*-th air chamber is

$$M_{Ai} = F_i \cdot L_i = F_i \cdot x_{iF}' \tag{24}$$

And the overall righting moment from air chambers is

$$M_A = \sum_{i=1}^{N} F_i \cdot x_{iF}' \tag{25}$$

3.3 Righting moment of the buoyancy tank

Let R_3, d be the external radius, draft of the buoyancy tank at the undisturbed floating state, respectively. The area of horizontal cross-section S_b can be written as

$$S_b = \pi(R_3^2 - R_2^2) \tag{26}$$

And the initial displacement of the buoyancy tank V_{BT0} is

$$V_{BT0} = S_b \cdot d \tag{27}$$

In the *O-xyz* coordinate system, the buoyancy center of the buoyancy tank is

$$x_{BT0} = 0, \quad y_{BT0} = 0, \quad z_{BT0} = -d/2 \tag{28}$$

Figure 7 portrays the transverse cross-section of the buoyancy tank. The water line moves to W_1W_2 at the new equilibrium state, which intersects with center line L at the point W and intersects with the external edge of buoyancy tank at points W_1 and W_2. $W_1'W_2'$goes through W and is vertical to L. $W_1'W_2'$ intersects with the external edge of the buoyancy tank at points

W_1' and W_2'. Let J_1, J_2 be the external, internal corner point, respectively, at the upper surface of the transverse cross-section of the buoyancy tank. Analogously, let J_3, J_4 be the external, internal corner point at the bottom surface, respectively.

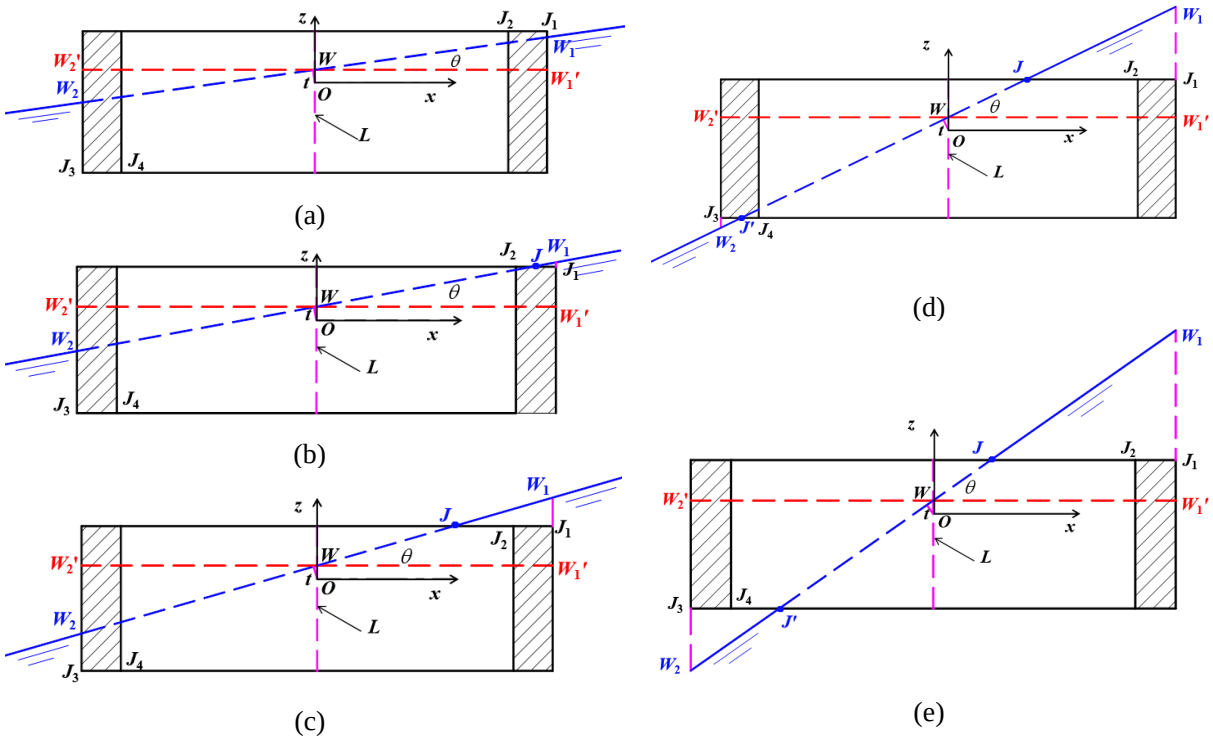

Figure 7. Transverse cross-section of the buoyancy tank

At the undisturbed floating state, the points J_1, J_2 stay in the air and J_3, J_4submerge in the water. With the increasing of the external moment M_E, the floating state of the buoyancy tank will experience the following 5 stages.

Stage-a: The trim angle is small, and points J_1, J_2 still stay in the air and J_3, J_4 still submerge in the water, as shown in Figure 7a.

Stage-b: A small part of the deck submerges in the water, i.e. J_2 still stays in the air and J_3, J_4 still submerge in the water, while J_1 submerges in the water, as shown in Figure 7b.

Stage-c: A significant part of the deck immersed into water, i.e. J_3, J_4 still submerge in the water, while both of J_1, J_2 submerges in the water, as shown in Figure 7c.

Stage-d: A small part of the bottom surfaces out of water, i.e. J_4 still submerges in the water, while J_3 surfaces out of water and J_1, J_2 submerge in the water, as shown in Figure 7d.

Stage-e: A significant part of the bottom surfaces out of water, i.e. J_3, J_4 surfaces out of water and J_1, J_2 submerge in the water, as shown in Figure 7e.

Let J, J' be the intersection points of the water line W_1W_2 and the deck, bottom of the buoyancy tank, respectively.

At the Stage-a, the geometry of the buoyancy tank under water is shown in Figure 8.

Obviously, the increase of displacement is

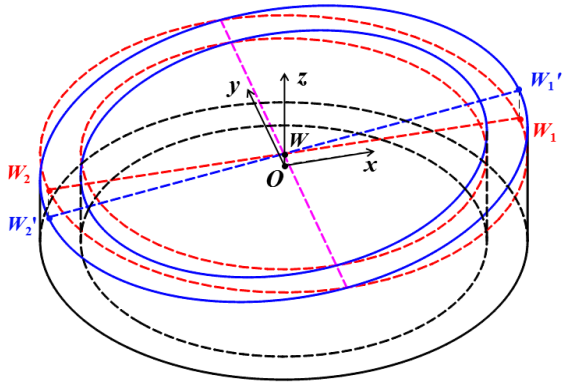

Figure 8. Sketch of the buoyancy tank under water at the Stage-a

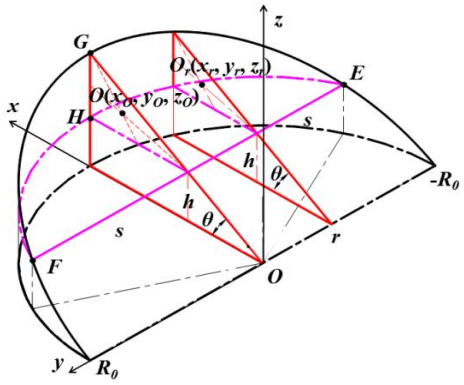

Figure 9. Sketch of oblique truncation of a cylinder

$$\Delta V_{\mathrm{BT}} = V_{\mathrm{BT}} - V_{\mathrm{BT0}} = S_b \cdot t / \cos\theta \tag{29}$$

In the *O-xyz* coordinate system, let (x_{BT}, 0, z_{BT}) be the buoyancy center of the buoyancy tank. In order to get x_{BT} and z_{BT}, the geometrical characteristics of a special structure *EGFHE* should be determined firstly, as shown in Figure 9. It is an oblique cut from a cylinder, the angle between the bottom surface *EFHE* and the slope surface *EFGE* is θ. Let R_0be the radius of cylinder, h the z-coordinate of the surface *EFHE*, s the half length of *EF*. According to geometrical relationship, one gets

$$s = \sqrt{R_0^{\,2} + h^2 - (h/\sin\theta)^2} \tag{30}$$

The volume of the structure *EGFHE* is the function of R_0, h and s, i.e. $V_{EGFHE}=f_V(R_0, h, s)$, which can be calculated by

$$f_V(R_0,h,s) = \int_{-s}^{s} dV = sR_0^{\,2}\tan\theta - \frac{1}{3}s^3\tan\theta - sh\sqrt{R_0^{\,2}-s^2} - hR_0^{\,2}\arcsin\frac{s}{R_0} + sh^2\cot\theta \tag{31}$$

where $dV = \frac{1}{2}[(R^2 - r^2)\cdot\tan\theta - 2h_0\sqrt{R^2 - r^2} + h_0^{\,2}\cot\theta]\cdot dr$.

Let ($f_x(R_0, h, s)$, $f_y(R_0, h, s)$, $f_z(R_0, h, s)$) be the buoyancy centre of *EGFHE*, which is also the function of R_0, h and s, and can be expressed as

$$\begin{cases} f_x(R_0,h,s) = \dfrac{\int_{-s}^{s} x_r dV}{V} = \dfrac{\mathrm{X}(R_0,h,s)}{f_V(R_0,h,s)} \\ f_y(R_0,h,s) = \dfrac{\int_{-s}^{s} y_r dV}{V} = 0 \\ f_z(R_0,h,s) = \dfrac{\int_{-s}^{s} z_r dV}{V} = \dfrac{\mathrm{Z}(R_0,h,s)}{f_V(R_0,h,s)} \end{cases} \tag{32}$$

where $\mathrm{X}(R_0,h,s)$ and $Z(R_0,h,s)$ are the function of R_0, h and s, and

$$\mathrm{X}(R_0,h,s)=\frac{s\cdot(5R_0^{\ 2}-2s^2)\sqrt{R_0^{\ 2}-s^2}\tan\theta}{12}+\frac{R_0^{\ 4}\tan\theta\arcsin\frac{s}{R_0}}{4}-shR_0^{\ 2}+\frac{s^3h+sh^3\cot^2\theta}{3}$$

$$Z(R_0,h,s)=\frac{s\cdot(5R_0^{\ 2}-2s^2)\sqrt{R_0^{\ 2}-s^2}\tan^2\theta}{24}+\frac{R_0^{\ 4}\tan^2\theta\arcsin\frac{s}{R_0}}{8}-\frac{sh^2\sqrt{R_0^{\ 2}-s^2}+h^2R_0^{\ 2}\arcsin\frac{s}{R_0}}{2}+\frac{2sh^3\cot\theta}{3}$$

Let (x_{g1}, y_{g1}, z_{g1}) and (x_{g2}, y_{g2}, z_{g2}) be the centroid of the triangle WW_1W_1' and WW_2W_2' in the *O-xyz* coordinate system, respectively. According to Eqs 31-32, one obtains their volume and centroid

$$V_{ww_1w_1'}=V_{ww_2w_2'}=f_V(R_3,0,R_3)-f_V(R_2,0,R_2)=\frac{2}{3}(R_3^{\ 3}-R_2^{\ 3})\cdot\tan\theta \tag{33}$$

$$\begin{cases} x_{g1}=-x_{g2}=\dfrac{f_V(R_3,0,R_3)\cdot f_x(R_3,0,R_3)-f_V(R_2,0,R_2)\cdot f_x(R_2,0,R_2)}{V_{ww_1w_1'}} \\ z_{g1}=\dfrac{f_V(R_3,0,R_3)\cdot f_z(R_3,0,R_3)-f_V(R_2,0,R_2)\cdot f_z(R_2,0,R_2)}{V_{ww_1w_1'}}+t/\cos\theta \\ z_{g2}=2t/\cos\theta-z_{g1} \end{cases} \tag{34}$$

And the buoyancy center of buoyancy tank in the *O-xyz* coordinate system should be

$$\begin{cases} x_{BT}=\dfrac{V_{ww_1w_1'}\cdot x_{g1}-V_{ww_2w_2'}\cdot x_{g2}}{V_{BT0}+\Delta V_{BT}} \\ z_{BT}=\dfrac{(V_{BT0}+\Delta V_{BT})\cdot(-d/2+t/2\cos\theta)+V_{ww_1w_1'}\cdot z_{g1}-V_{ww_2w_2'}\cdot z_{g2}}{V_{BT0}+\Delta V_{BT}} \end{cases} \tag{35}$$

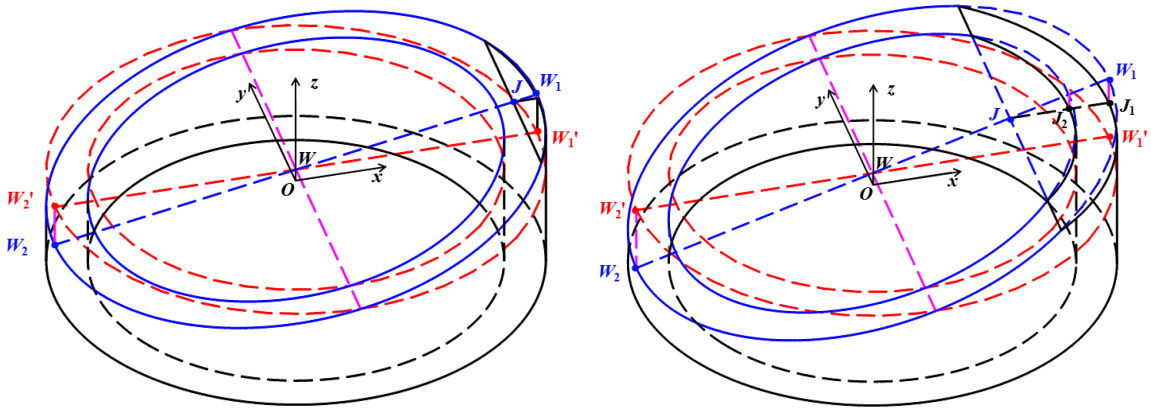

Figure 10. Sketch of the buoyancy tank under water at the Stage-b (a) and Stage-c (b)

At the Stage-b, the shape of the buoyancy tank under water is shown in Figure 10a. The increase of displacement can be written as

$$\Delta V_{\mathrm{BT}} = S_b \cdot t/\cos\theta - V_{W_1JJ_1} = S_b \cdot t/\cos\theta - f_V(R_3, h_1, s_1) \tag{36}$$

where $h_1 = z_{f0} - t/\cos\theta$, $s_1 = \sqrt{R_3^{\,2} + h_1^{\,2} - (h_1/\sin\theta)^2}$.

Let (x_{g3}, y_{g3}, z_{g3}) be the centroid of the triangle W_1JJ_1 in the *O-xyz* coordinate system. According to Eqs 33-34, one gets

$$x_{g3} = f_x(R_3, h_1, s_1), \quad z_{g3} = f_z(R_3, h_1, s_1) \tag{37}$$

Analogously, at the Stage-c (see Figure 10b) one obtains the increase of displacement and the centroid of the triangle W_1JJ_1 in the *O-xyz* coordinate system

$$\Delta V_{\mathrm{BT}} = S_b \cdot t/\cos\theta - f_V(R_3, h_1, s_1) + f_V(R_2, h_1, s_2) \tag{38}$$

$$\begin{cases} x_{g3} = \dfrac{f_V(R_3,h_1,s_1)\cdot f_x(R_3,h_1,s_1) - f_V(R_2,h_1,s_2)\cdot f_x(R_2,h_1,s_2)}{f_V(R_3,h_1,s_1) - f_V(R_2,h_1,s_2)} \\ z_{g3} = \dfrac{f_V(R_3,h_1,s_1)\cdot f_z(R_3,h_1,s_1) - f_V(R_2,h_1,s_2)\cdot f_z(R_2,h_1,s_2)}{f_V(R_3,h_1,s_1) - f_V(R_2,h_1,s_2)} \end{cases} \tag{39}$$

where $s_2 = \sqrt{R_2^{\,2} + h_1^{\,2} - (h_1/\sin\theta)^2}$.

In Stage-b and Stage-c, the buoyancy center of buoyancy tank in the *O-xyz* coordinate system should be

$$\begin{cases} x_{Bt} = \dfrac{V_{WW_1W_1'}\cdot x_{g1} - V_{WW_2W_2'}\cdot x_{g2} - V_{W_1JJ_1}\cdot x_{g3}}{V_{BT0} + \Delta V_{BT}} \\ z_{BT} = \dfrac{(V_{BT0} + \Delta V_{BT})\cdot(-d + t/\cos\theta)/2 + V_{WW_1W_1'}\cdot z_{g1} - V_{WW_2W_2'}\cdot z_{g2} - V_{W_1JJ_1}\cdot z_{g3}}{V_{BT0} + \Delta V_{BT}} \end{cases} \tag{40}$$

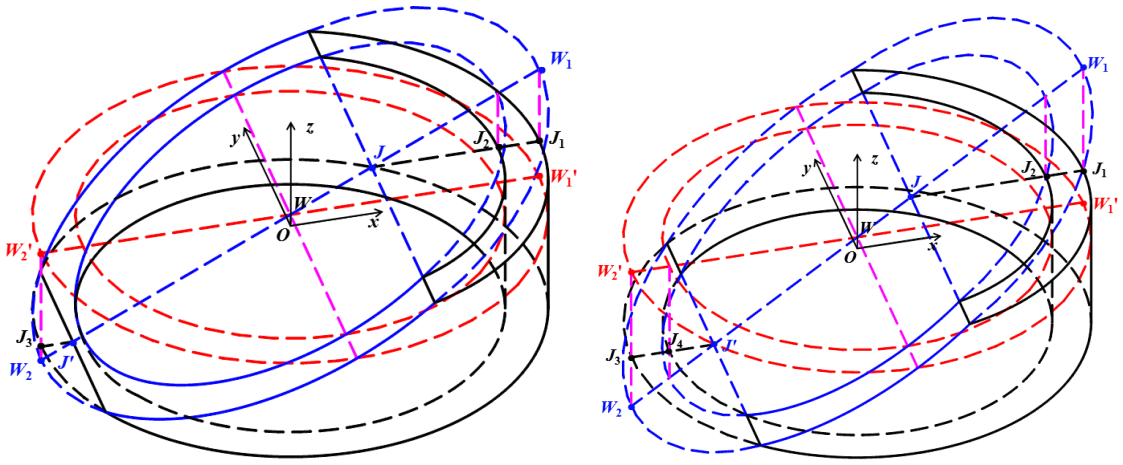

(a) (b)

Figure 11. Sketch of the buoyancy tank under water at the Stage-d (a) and Stage-e (b)

At the Stage-d (see Figure 11a), the increase of displacement can be written as

$$\begin{aligned}\Delta V_{\mathrm{BT}} &= S_b \cdot t/\cos\theta - V_{W_1JJ_1} + V_{W_2J'J_3} \\ &= S_b \cdot t/\cos\theta - f_V(R_3,h_1,s_1) + f_V(R_2,h_1,s_2) + f_V(R_3,h_2,s_3)\end{aligned} \tag{41}$$

where $h_2 = d + t/\cos\theta$, $s_3 = \sqrt{R_3^{\,2} + h_2^{\,2} - (h_2/\sin\theta)^2}$.

Let (x_{g4}, y_{g4}, z_{g4}) be the centroid of the triangle $W_2J'J_3$ in the *O-xyz* coordinate system. According to Eqs 33-34, the coordinate is

$$x_{g4} = f_x(R_3,h_2,s_3), \quad z_{g4} = f_z(R_3,h_2,s_3) \tag{42}$$

Analogously, at the Stage-e (see Figure 11b) one has the increase of displacement and the centroid of the triangle $W_2J'J_3$ in the *O-xyz* coordinate system

$$\Delta V_{\mathrm{BT}} = S_b \cdot t/\cos\theta - f_V(R_3,h_1,s_1) + f_V(R_2,h_1,s_2) + f_V(R_3,h_2,s_3) - f_V(R_2,h_2,s_4) \tag{43}$$

$$\begin{cases} x_{g4} = \dfrac{f_V(R_3,h_2,s_3)\cdot f_x(R_3,h_2,s_3) - f_V(R_2,h_2,s_4)\cdot f_x(R_2,h_2,s_4)}{f_V(R_3,h_2,s_3) - f_V(R_2,h_2,s_4)} \\ z_{g4} = \dfrac{f_V(R_3,h_2,s_3)\cdot f_z(R_3,h_2,s_3) - f_V(R_2,h_2,s_4)\cdot f_z(R_2,h_2,s_4)}{f_V(R_3,h_2,s_3) - f_V(R_2,h_2,s_4)} \end{cases} \tag{44}$$

where $s_4 = \sqrt{R_2^{\,2} + h_2^{\,2} - (h_2/\sin\theta)^2}$.

In Stage-d and Stage-e, the buoyancy center of buoyancy tank in the *O-xyz* coordinate system should be

$$\begin{cases} x_{BT} = \dfrac{V_{WW_1W_1'}\cdot x_{g_1} - V_{WW_2W_2'}\cdot x_{g_2} - V_{W_1JJ_1}\cdot x_{g_3} + V_{W_2J'J_3}\cdot x_{g_4}}{V_{BT0} + \Delta V_{BT}} \\ z_{BT} = \dfrac{(V_{BT0} + \Delta V_{BT})\cdot(-d + t/\cos\theta)/2 + V_{WW_1W_1'}\cdot z_{g_1} - V_{WW_2W_2'}\cdot z_{g_2} - V_{W_1JJ_1}\cdot z_{g_3} + V_{W_2J'J_3}\cdot z_{g_4}}{V_{BT0} + \Delta V_{BT}} \end{cases} \tag{45}$$

Let (x_{BT}', y_{BT}', z_{BT}') be the buoyancy center of the buoyancy tank in the *O-x'y'z'* coordinate system. The total contribution of the buoyancy tank to righting moment is

$$M_{BT} = \rho g \cdot V_{BT} \cdot x_{BT}' = \rho g \cdot (V_{BT0} + \Delta V_{BT}) \cdot (x_{BT} \cdot \cos\theta + z_{BT} \cdot \sin\theta) \tag{46}$$

At the Stage-e, however, air could leak from the air chamber adjacent to point J_4, which makes the air chamber lose buoyancy. Assuming that the *k*th air chamber leaks out, then we get $z_{ak}' = t$, and an extra condition should be imposed on Eq 6. The modified Eq 6 is

$$P_{0i}V_{0i} = P_iV_i \qquad (i \neq k) \tag{47}$$

4. Numerical results

4.1 Verification of the new analytical method

To verify the analytical method presented in the last section, the commercial CFD software Star-CCM+ [29] was employed for comparison. The numerical results are shown in Figure 12,

where the solid line is the result from the analytical method and the black points are the results from Star-CCM+. One can observe that the solid line agrees very well with black points when the trim angle is less than 38°. One can also note that when the trim angle is larger than 38°, discrepancy between two results appears and gradually increases. This is because the wetted surface in air chambers submerges in water under very large trim angles, which is not considered in the analytical model in this paper. Nevertheless, under very large trim angles, the ACBP-OWT system nearly completely loses righting moment and thus it makes no sense to precisely predict the stability under such situation. Therefore, the presented analytical method is appropriate for the stability analysis of the ACBP-OWT system.

In Figure 12, $S_1(\theta_1=12.6^o)$, $S_2(\theta_2=16.09^o)$, $S_3(\theta_3=19.2^o)$, $S_4(\theta_4=25.6^o)$ are the 4 critical states, at which the upper corner point J_1 or J_2 starts to submerge into water, or the bottom corner point J_3 or J_4 starts to surface out of water. In other words, S_1, S_2, S_3, S_4 are the critical states between each pair of adjacent floating stages (Stage-a~Stage-e). From the figure one notices that the righting moment linearly increases before critical state S_1, and then smoothly increases with a gradually decreasing growth rate when passing through S_1, S_2, S_3 until reaches its maximum at $\theta_m=23^o$. After that, the righting moment gradually decreases until state S_4, at which the air chamber adjacent to J_4 starts to leak out and its buoyancy suddenly completely loses. As a result, the righting moment falls sharply. After state S_4, the righting moment almost linearly decreases with the trim angle and the stability completely loses at $\theta=46^o$. One might also observe that there is a slightly jump on the righting moment at $\theta=44^o$, which suggests that more air chambers leak out. It is worth mentioning that the air chambers that leak out at $\theta=44^o$ do not contribute much to the righting moment due to the fact that the arm of righting force is very short.

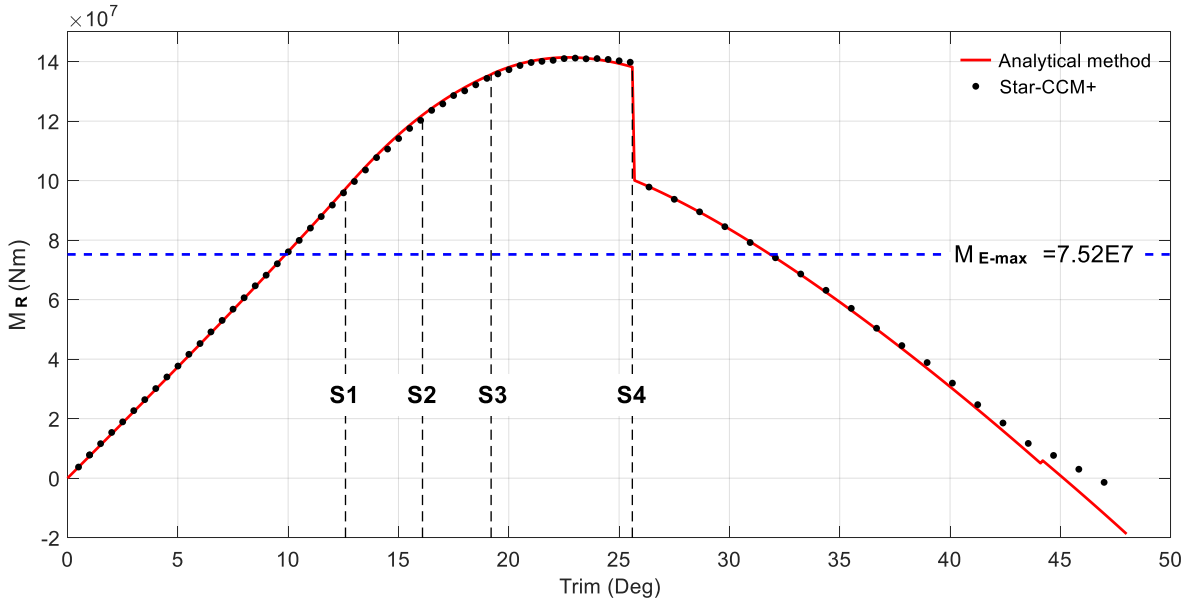

Figure 12. Righting moment M_R against the trim angle

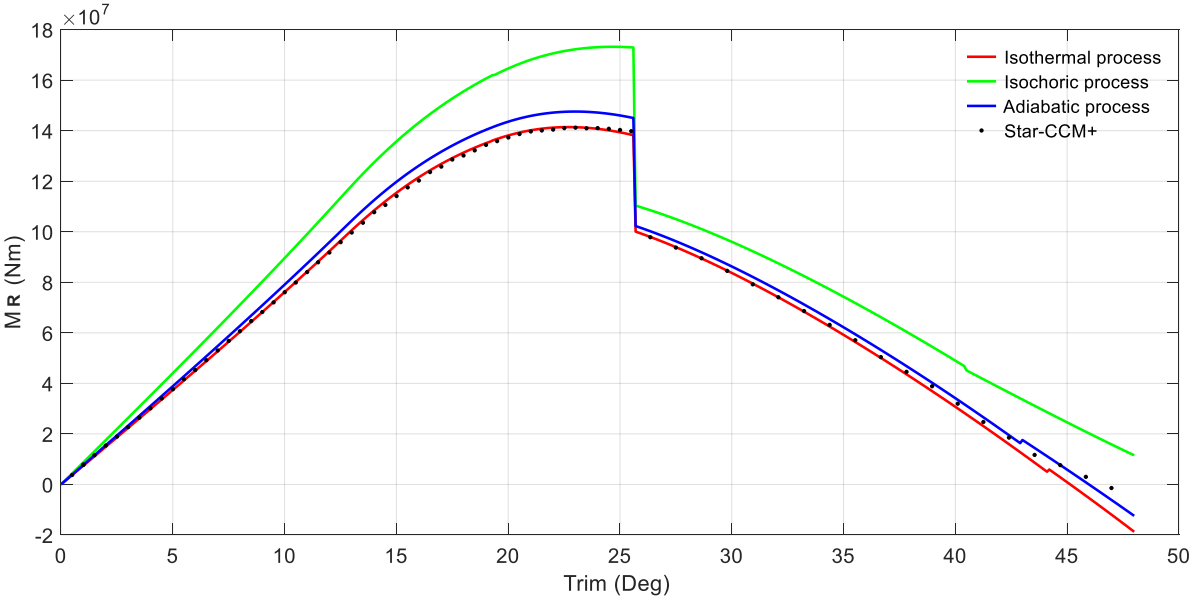

Figure 13. Righting moment M_R against the trim angle in different compression model

Figure 13 shows the righting moment of ACBP-OWT in different compression models. The red, green and blue lines are the results of isothermal process, isochoric process and adiabatic process. As shown above, the results of isothermal process agree well with CFD results, which means the compression model is reasonable and the compressible of gas in air chamber cannot be ignored. If the internal gas is considered incompressible, the results will be the green line that is larger than the CFD results. By this way, the safety factor in stability assessment will be larger, which is dangerous in practical application. The adiabatic process model has slightly different results as compared to the isothermal or CFD simulation ones,

which might be more appropriate for the dynamic stability analysis due to insufficient heat exchange. In a word, the gas in ACBP-OWT system must be considered compressible, which is different to the third type of damage stability, and the compression model can be considered as isothermal process in the static stability analysis.

According to Table 2, the rated wind speed of the NREL-5MW Offshore Wind Turbine is 11.4m/s, and the resulting maximum wind load thrust is 800kN that acts on the wind turbine hub[28]. So the maximum external moment from the wind load is

$$M_{E-\max} = T_{\max} \cdot (H_{hub} + z_{f0}) = 7.52 \times 10^{7} (N \cdot m) \tag{48}$$

It is speculated that the wind turbine will lose substantial efficiency when the trim angle is beyond 10^{o} [27]. In this case, the righting moment of the ACBP-OWT system is $7.61 \times 10^{7} N.m$ at $\theta = 10^{o}$, which is sufficient to balance the maximum wind load $M_{E\text{-}max}$. It is also worth mentioning that the ACBP-OWT system is about 1800 tons lighter than the MIT/NREL SDB [27], which can greatly reduce the material cost of the system.

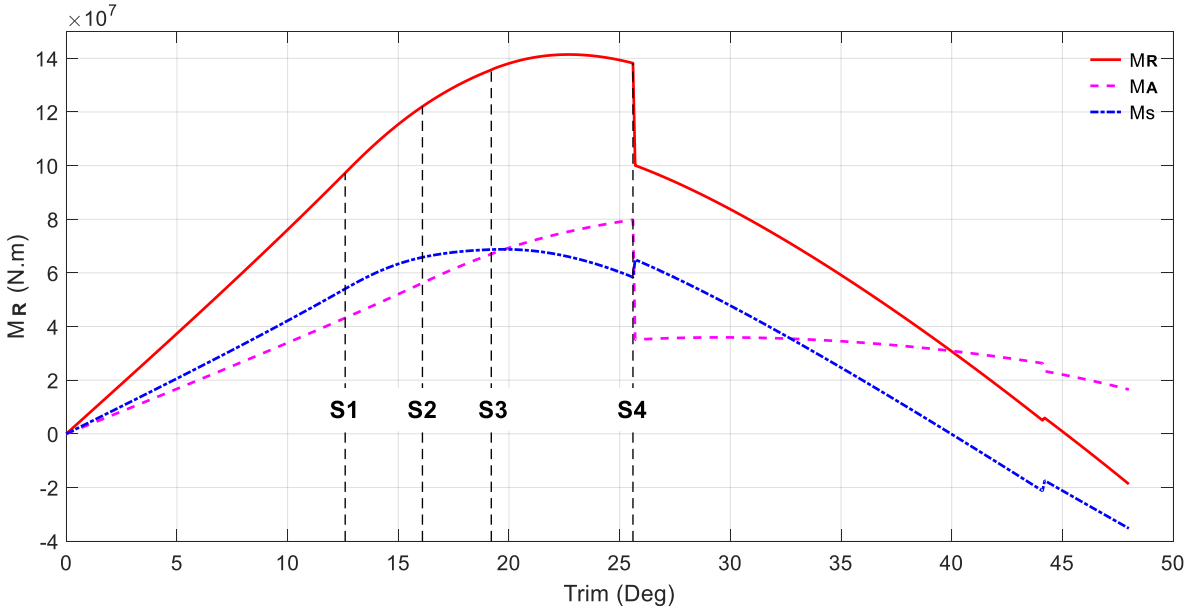

Figure 14. The contribution from air cushion M_A, the displacement and weight of structures M_S to the righting moment M_R

4.2 Contribution from structures and air cushion to the righting moment

The total righting moment of the ACBP-OWT system is contributed by the structures and air cushion, which are shown in Figure 14. In the figure, the solid, dashed, dash-dotted line are the total righting moment, air cushion righting moment, righting moment due to the displacement and weight of structures, respectively. S_1, S_2, S_3, S_4 are the 4 critical states that are the same as those in Figure 12. It can be seen that the dashed line is always beyond the

horizontal axis, which suggests that the air cushion always makes positive contribution to righting moment. In contrast, the dash-dotted line is below the horizontal axis when trim angle θ>40°, which reveals that the structures can contribute negative righting moment at large trim angles. One can find that the air cushion righting moment almost linearly increases with the trim angle until air leaks out, after which the air cushion righting moment slowly decreases with the trim angle. In contrast, the righting moment due to the displacement and weight of structures smoothly increases with a gradually decreasing growth rate when passing through S_1, S_2, S_3 until θ=19.5°, and then quickly decreases with the trim angle. One can also notice that there are two jumps occurring on the righting moment due to the displacement and weight of structures when air leaks out from chambers, which is due to the change of the buoyancy from structures when the internal free surface falls to the external one.

The sinkage of the ACBP-OWT system is shown in Figure 15. Obviously, the sinkage is very small and can be ignored before the critical state S_2. After that, the ACBP-OWT system sinks down approximately linearly with the trim angle. Then the sinkage has a significant jump at the critical state S_4, which means that the air chambers from which air leaks out provide negative buoyancy. Simultaneously, the sinkage jump makes the center of buoyancy move to a new position and causes a jump on M_S.

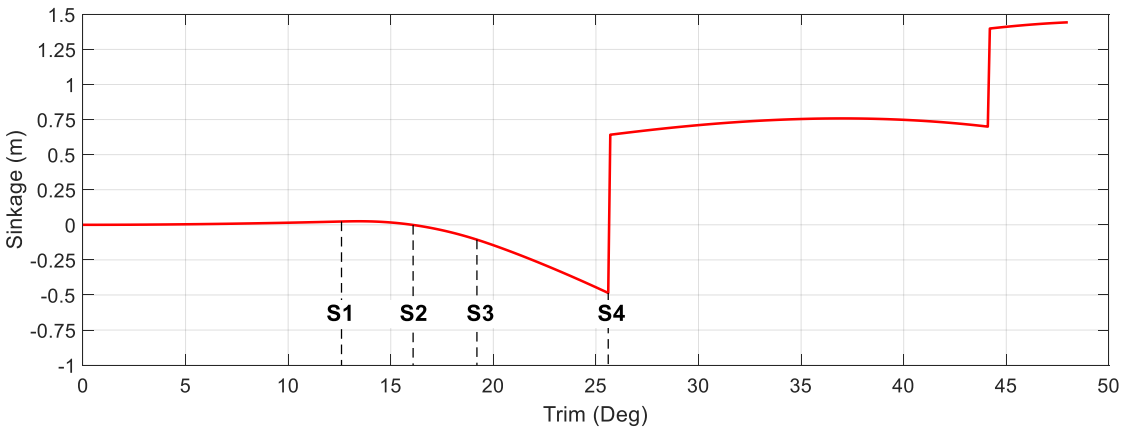

Figure 15. The sinkage of the ACBP-OWT system

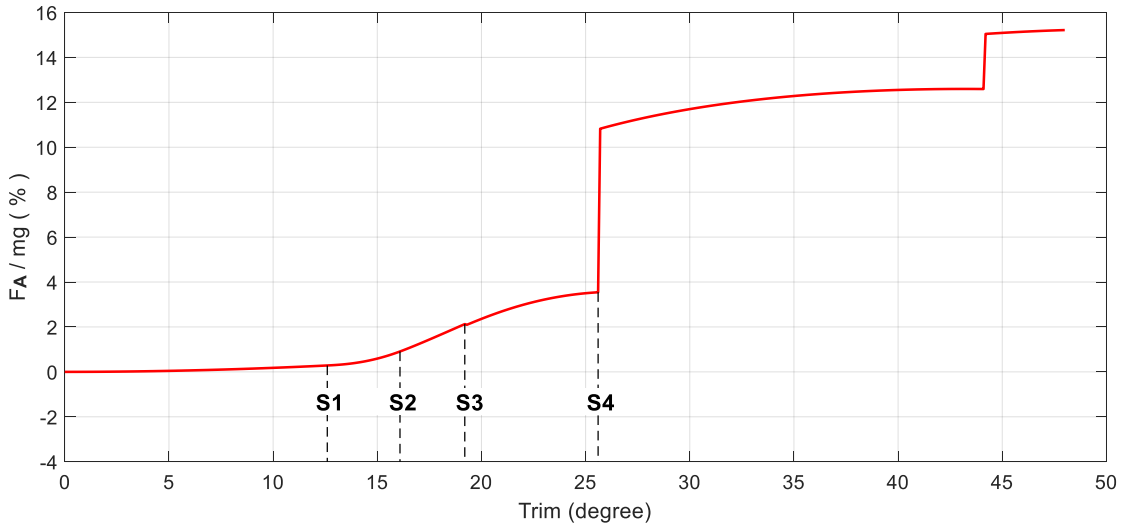

Figure 16. The proportion of the air cushion displacement F_A to the ACBP-OWT displacement mg

Figure 16 depicts the proportion of the air cushion displacement F_A to the ACBP-OWT displacement mg. The initial displacement of air cushion is zero, which is given by setting the altitude of the free surface in air cushions as z_{a0}=0 (see Table 1). When the trim angle is small (θ<12.5°), the proportion F_A/mg is extremely small and increases very slowly. After the critical state S_1, the proportion F_A/mg increases quickly with the trim angle, which suggests the displacement from structures is decreasing. At the critical state S_4, air leaks out from a chamber and its negative buoyancy suddenly changes to zero, which makes the proportion F_A/mg jump from 3.8% to a significant value 11%. After that, the proportion F_A/mg still slowly increases with the trim angle and gets another jump when air leaks out from more chambers.

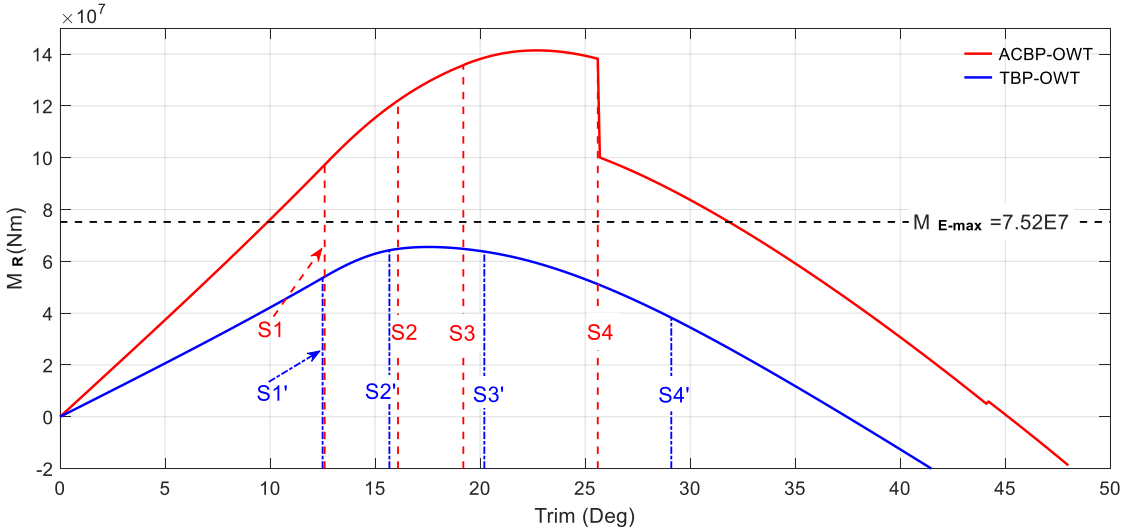

Figure 17. Righting moment of ACBP-OWT and TBP-OWT against trim angle

4.3 Comparison of righting moment between ACBP-OWT and TBP-OWT

According to the above analysis, the newly presented ACBP-OWT shows good stability performance, in which the air cushion plays an important role. To demonstrate it, the function of the air cushion is disabled by removing the top surface of air chambers from the ACBP-OWT system. For simplicity, the ACBP-OWT system without air cushion is called the TBP-OWT (Traditional Barge Platform Offshore Wind Turbine) system. Since the displacement of the air cushion in the ACBP-OWT system is zero, the total displacement of the TBP-OWT system is the same as the ACBP-OWT one (the mass of the top surface of air chambers was neglected). Figure 17 shows the righting moment of the TBP-OWT system (blue line) against trim angle, as compared with that of the ACBP-OWT system (red line). It is obviously that the righting moment of the ACBP-OWT system is significantly larger than the TBP-OWT system, and the latter is much earlier to lose stability. It is interesting that the critical states S'_1, S'_2 for the TBP-OWT system arrive a little earlier than S_1, S_2 for the ACBP-OWT system, while S'_3, S'_4 arrive significantly later than S_3, S_4. The discrepancies between S_i and S'_i (i=1~4) are due to the influence of air cushion.

Besides, the maximum righting moment of the TBP-OWT system is $6.55\times10^7 N.m$ at θ=17.5°, which is smaller than the maximum wind load $M_{E\text{-}max}$. In order to obtain larger righting moment, the physical dimension of the TBP should be upscaled, which inevitably makes its displacement and manufacturing cost increase. Therefore, the air cushion can greatly increase the righting moment of the ACBP, as well as the stability of the ACBP-OWT system.

4.4 Dynamic stability of ACBP-OWT

The above is the preliminary static design of ACBP-OWT, in which the principal dimensions are referred to the MIT/NREL SDB [27] and the performance of static stability is studied. In order to obtain good dynamic performance, the ACBP need to be upscaled. For floating wind turbine, the mean and maximum trim angle in operating state should be less than 5 and 10 degrees []. According to the law of similarity, the upscale factor is about 1.125 and the principal parameters of upscaled ACBP is shown in Table 3.

Table 3. The principal parameters of the upscaled ACBP

Internal radius of air cushion R_1	6.3 m	Installed draft	22.5 m
External radius of air cushion R_2	15.75 m	Buoyancy tank draft d	6.953 m
External radius of buoyancy tank R_3	20.25 m	Number of air chambers	8
Radius of ballastR_4	22.5 m	Ballast mass	2,847,656 kg
Radius of damping skirt	22.5 m	Total mass	4,146,000 kg

Deck clearance z_{f0}	4.5 m	COG of ACBP	(0.0, 0.0, -16.48) m
Free Surface in air cushion z_{a0}	0.0 m	COG of ACBP-OWT	(0.0, 0.0, -4.323) m

*COG is the center of gravity

The work done by righting moment or external one, which can be depicted by the curve of dynamic stability, is obtained by the integral of static stability curve over the trim angle [16][30].

If the wind load is considered solely and the effect of wave is ignored, the ACBP-OWT will pitch from zero angle and the works done by righting moment and wind heeling moment are shown in Figure 18.

The red solid line is the work of righting moment, which is obtained by

$$W_R(\theta) = \int_0^\theta M_R d\theta \tag{49}$$

It is worth noting that, since the pitch is fast and heat exchange is insufficient, the adiabatic law is employed in dynamic stability analysis, which would be more appropriate than the isothermal one.

The blue solid line is the work of wind heeling moment at rated wind speed, according to [28], at which the maximum wind load thrust of NREL-5MW Offshore Wind Turbine is obtained. Assuming that the trim angle of ACBP-OWT is zero, the thrust can be obtained by

$$T_{\max} = 0.5\rho V_{rated}{}^2 S_0 \cdot C_T = 0.5\rho V_{rated}{}^2 (0.25\pi D_{rotor}{}^2) \cdot C_T \tag{50}$$

where V_{rated} is the rated wind speed, S_0 is windward area of wind turbine and C_T is the thrust coefficient of wind turbine at V_{rated}.

If the ACBP-OWT has a trim angle, the wind load thrust of wind turbine will be

$$T_r(\theta) = 0.5\rho V_{rated}{}^2 S \cdot C_T = 0.5\rho V_{rated}{}^2 (S_0 \cdot \cos\theta) \cdot C_T = T_{\max} \cdot \cos\theta \tag{51}$$

In which, S is the windward area of wind turbine at this moment.

The wind load thrust acts on the hub of wind turbine, its arm and wind heeling moment in the $O\text{-}x'y'z'$ coordinate system will be

$$l_T = (H_{hub} + z_{f0}) \cos\theta \tag{52}$$

$$M_{W-r}(\theta) = T_r(\theta) \cdot l_T = T_{\max} \cdot (H_{hub} + z_{f0}) \cos^2\theta \tag{53}$$

Then the work done by wind load thrust at rated wind speed can be obtained by integrating the wind heeling moment with respect to trim angle

$$W_{W-r}(\theta) = \int_0^\theta M_{W-r} d\theta = T_{\max} \cdot (H_{hub} + z_{f0}) \cdot (0.5\theta + 0.25\sin 2\theta) \tag{54}$$

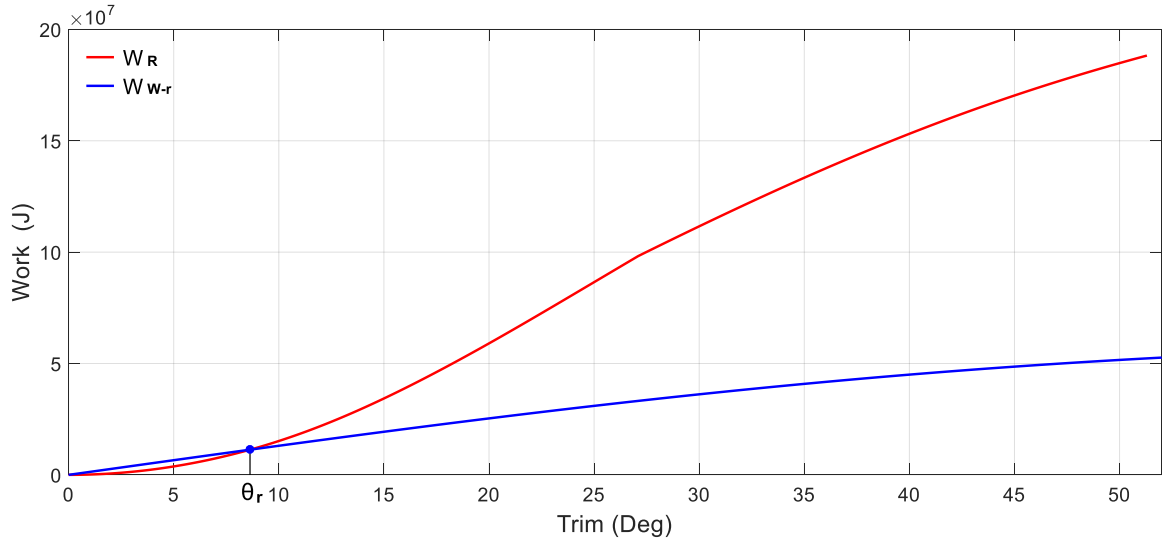

Figure 18. Dynamic stability curve of ACBP-OWT against trim angle without effect of wave

The blue solid line intersects with the red one at θ_r=8.63°, which is solved by $W_R(\theta)=W_{W\text{-}r}(\theta)$. According to [16][30], it means that the works done by them are the same, and the angular velocity of trim at that point is zero. When the trim angle is 8.63°, the angular velocity of trim is zero and the righting moment of ACBP-OWT is larger than the moment of wind load at this state. Consequently the ACBP-OWT will have surplus righting moment to help itself return to the equilibrium position θ=4.33°, which is solved by $M_R(\theta)=M_{W\text{-}r}(\theta)$. It means that the ACBP-OWT is in stable dynamic equilibrium state and the maximum dynamic trim angle in rated wind speed is 8.63°, which meets the requirements of floating wind turbine in operating state.

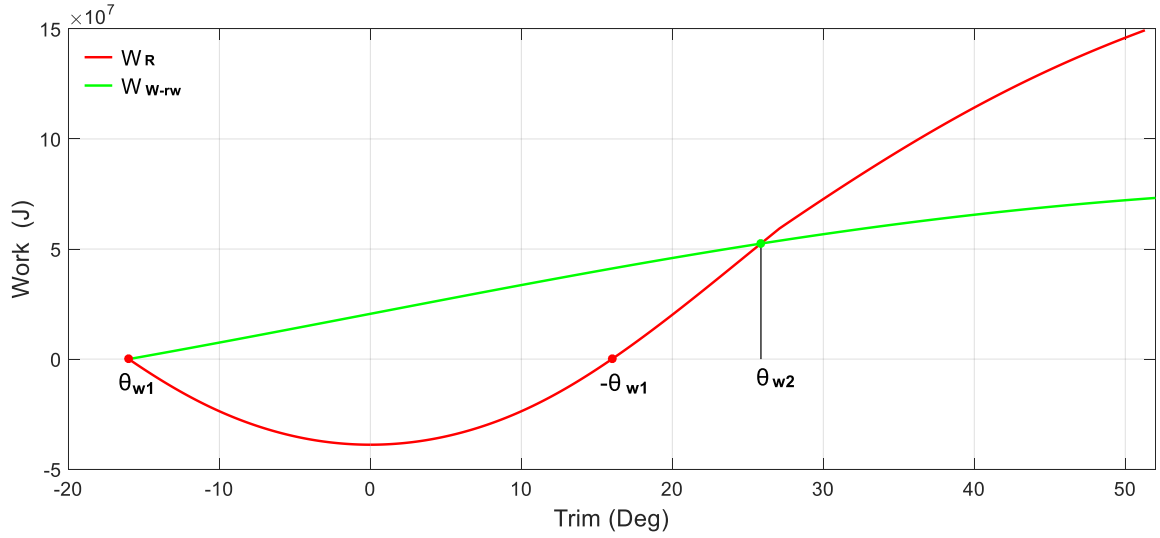

Figure 19. Dynamic stability curve of ACBP-OWT against trim angle in weather criterion

If the effect of wave is taken into consideration, according to the weather criterion of [31], the ACBP-OWT will have an angle of pitch to windward due to wave action, and the angle

should not exceed 16°. In this case, the worst case is considered, i.e. the pitch angle $|\theta_{w1}|$ due to wave action is 16° at the rated wind speed and the ACBP-OWT makes pitch motion from the negative angle $\theta=\theta_{w1}<0$ rather than zero. As shown in Figure 19, the red and green solid lines are the works done by righting moment and wind heeling moment, which are obtained by

$$W_{R\text{-}w}(\theta)=\int_{\theta_{w1}}^{\theta} M_R(\theta)d\theta=\begin{cases}\int_{\theta_{w1}}^{\theta} -M_R(-\theta)d\theta & \theta\le 0\\ \int_{\theta_{w1}}^{0} -M_R(-\theta)d\theta+\int_{0}^{\theta} M_R(\theta)d\theta & \theta>0\end{cases} \tag{59}$$

$$W_{W-rw}(\theta)=\int_{\theta_{w1}}^{\theta} M_{W-r}d\theta=T_{\max}\cdot(H_{hub}+z_{f0})\cdot[0.5(\theta-\theta_{rw1})+0.25(\sin 2\theta-\sin 2\theta_{rw1})] \tag{60}$$

The two lines begin from θ_{rw1}= -16° and intersect with each other at θ_{rw2}= 25.87°, which is solved by $W_{R\text{-}w}(\theta)=W_{W\text{-}rw}(\theta)$. The righting moment does the negative work when trim angle is less than zero and the total work becomes positive after the trim angle is larger than $-\theta_{w1}$. The righting moment does the same work to wind heeling moment when $\theta=\theta_{rw2}$, meanwhile, the ACBP-OWT is in stable dynamic equilibrium state and can return to the equilibrium position.

For the upscaled ACBP-OWT, the air escaping will occur after the trim angle is more than 27.1°, which is larger than θ_{rw2} and the upscaled ACBP-OWT can meet the requirements of the weather criterion of [31].

5. Conclusions and Discussions

The concept of Air cushion Barge Platform (ACBP) is proposed, which incorporates multiple air chambers, used for supporting an Offshore Wind Turbine (OWT). To evaluate the stability of the system, a new analytical method is presented in this paper, which can analyze the stability of a multi-air cushion structure. The method is validated by the CFD results. Then the characteristics of the static and dynamic stability of the ACBP-OWT system is investigated using this method, and the following observations are demonstrated.

1) For analyzing the static stability of the ACBP-OWT structure at large trim angles, the isothermal air model achieves desirable results as compared to the CFD ones. In contrast, the adiabatic law is more appropriate in the dynamic stability analysis.

2) The air cushion always makes considerable positive contribution to the righting moment, but it will suffer great loss if the air leaks from cushions at very large trim angles. In contrast, the structure can provide negative righting moment at large trim angles.

3) The righting moment provided by air cushions decreases much more slowly than the one due to the displacement and weight of structures at large trim angles.

4) Although the displacement due to air chambers can be set at zero in the undisturbed floating state, the air chambers provide significant righting moment with increase in the trim angle, making the system to be more stable at the whole range of angles compared with the designs without the air chambers.

5) The dynamic trim angle at rated wind load is much less than the trim angle of maximum righting moment, which suggests the ACBP-OWT is stable under the working conditions.

It is noted that the principle of the method for stability analysis can be applied to other type of air cushion structures, thought the specific equations may be different.

Acknowledgments

This work is supported by the National Natural Science Foundation of P.R. China (51739001 and 51579056) and the Natural Science Foundation of Heilongjiang Province of China (Grant No. E2018025).

References

[1] Wang CM, Utsunomiya T, Wee SC, Choo YS. Research on floating wind turbines: a literature survey. The IES Journal Part A: Civil & Structural Engineering. 2010;3(4):267-277.

[2] Utsunomiya T, Matsukuma H, Minoura S, Ko K, Hamamura H, Kobayashi O, Sato I, Nomoto Y, Yasui K. At Sea Experiment of a Hybrid Spar for Floating Offshore Wind Turbine Using 1/10-Scale Model. J. Offshore mech. Art. Eng. 2013;135(3):1-8.

[3] Jonkman JM. Dynamics Modeling and Loads Analysis of an Offshore Wind Turbine. NREL Technical Report No. TP-500-41958. November, 2007.

[4] Borg M, Ortigado EU, Collu M, Brennan FP. Passive damping systems for floating vertical axis wind turbines analysis. European wind energy Conference: Proceedings. Vienna, Austria, EWEA, 3-7 Feb., 2013.

[5] Luo N, Bottasso CL, Karimi HR, Zapateiro M. Semi active Control for Floating Offshore Wind Turbines Subject to Aero-hydro Dynamic Loads. International Conference on Renewable Energies and Power Quality (ICREPQ'11): Proceedings. Las Palmas de Gran Canaria (Spain), 13th to 15th April, 2011.

[6] Luo N, Pacheco L, Vidal Y, Li H. Smart structural control strategies for offshore wind power generation with floating wind turbines. International Conference on Renewable Energies and power Quality: Proceedings. Santiago de Compostela, Spain, 28-30 March,

2012.

[7] Shadman M, Akbarpour A. Comparative study of utilizing a new type V-shaped Tuned Liquid Column Damper and U-shaped Tuned Liquid Column Damper in floating wind turbines. The ASME 31st International Conference on Ocean, Offshore and Arctic Engineering: Proceedings. Rio de Janeiro, Brazil, ASME, 1-6 July, 2012.

[8] Shadman M, Akbarpour A.Utilizing TLCD (Tuned Liquid ColumnDamper) in floating wind turbines. The ASME 31stInternational Conference on Ocean,Offshore and Arctic Engineering: Proceedings.Rio de Janeiro, Brazil, ASME, 1-6 July, 2012.

[9] Lackner MA, Rotea MA. Structural control of floating wind turbines. Mechatronics. 2011;21(2011):704-719.

[10] Patel MH, Harrison JH. The mechanics of a compliant motion suppression system for semi-submersibles. Journal of Sound and Vibration. 2002;106(3):491-507.

[11] Pinkster JA, Meevers Scholte EJA. The behaviour of a large air-supported MOB at sea. Marine Structures. 2001;14(2001):163-179.

[12] Kessel JV, Pinkster JA. The Effect of Air cushion Division on The Structural Loads of Large Floating Offshore Structures. Proceedings of the 26th International Conference on Offshore Mechanics and Arctic Engineering, San Diego, California, 10-15 Jane, 2007.

[13] Burns G et al. Dynamic submergence analysis of the khazzan dubai subsea oil tanks. Paper No.OTC1667, Proceedings of the Offshore Technology Conference, Houston, 1972.

[14] Kure G, Lindaas OJ. Record-breaking air lifting operation on the gullfaks C project. Paper No.OTC5775, Proceedings of the Offshore Technology Conference, Houston, 1988.

[15] Berthin JC, Hudson WL, Doris CG, Mirabo DO. Installation of maureen gravity platform over atemplate. Paper No.OTC 4876, Proceedings of the Offshore Technology Conference, Houston, 1985.

[16] Sheng ZB, Liu YZ. Ship Statics. Shanghai Jiao Tong University Press. 2003.

[17] Bie SA, Ji CN, Ren ZJ, Li ZZ. Study on Floating Properties and Stability of Air Floated Structures. China Ocean Engineering, 2002;16(2):263-272.

[18] Bie SA, Xu YL, Wang GL. Static stability analysis of air floated structures. J Tsinghua Univ (Sci & Tech). 2002;42(2):274-277.

[19] Ding HY, Zhao X, Le CH, Zhang PY, Min QL. Towing Motion Characteristics of Composite Bucket Foundation for Offshore Wind Turbines. Energies.

2019;19(12):37-67.

[20] Liu XQ, Zhang PY, Zhao MJ, Ding HY, Le CH. Air-Floating Characteristics of Large-Diameter Multi-Bucket Foundation for Offshore Wind Turbines. Energies. 2019;21(12):41-58.

[21] Liu XQ, Zhang PY, Zhao MJ, Ding HY, Le CH. Influencing Factors of Motion Responses for Large-Diameter Tripod Bucket Foundation. Applied Sciences. 2019;22(9):49-57.

[22] Chenu B, Morris-Thomas MT, Thiagarajan KP. Some hydrodynamic characteristics of an air cushion supported concrete gravity structure. 15th Australasian Fluid Mechanics Conference, 13-17 December, 2004.

[23] Thiagarajan, K.P. Hydrostatic stability of compartmented structures supported by air cushions. J. Ship Res.2009;53(3):151–158.

[24] KesselJV. Air cushion supported Mega-Floaters. PhD thesis, Delft University of Technology. 2010.

[25] Ma QW, Patel MH. Coupled nonlinear motion of floating structures with water columns in open-bottom tanks. The International Conference on Offshore Mechanics and Arctic Engineering (OMAE): Proceedings. Oslo, Norway, 23-28 June, 2002.

[26] Bie SA, Ren ZJ, Li ZZ. Mechanical Properties of Air Floating Structures. Chinese Journal of Applied Mechanics. 2004;21(4):68-71.

[27] Wayman EN, Sclavounos PD, Bytterfield S, Jonkman J, Musial W. Coupled Dynamics Modeling of Floating Wind Turbine Systems. Offshore Technology Conference: Proceedings. Houston, Texas, 1-5 May, 2006.

[28] Jonkman J, Butterfield, S, Musial W, Scott G. Definition of a 5-MW Reference Wind Turbine for Offshore System Development. NREL/TP-500-38060, Golden, CO: National Renewable Energy Laboratory, January 2009.

[29] Siemens. User manual: Star-CCM+ V12.02.010. 2017.

[30] CSSC, CSIC, CSNAME. Practical manual for Ship Design - General Design. National Defence Industry Press. 2013.

[31] IMO, MSC. International Code On Intact Stability. 2008.